RESEARCH ARTICLE

Characterization of a compact piezoelectric actuated microgripper based on double-stair bridge-type mechanism

Tilok Kumar Das[1] · Bijan Shirinzadeh[1] · Mohammadali Ghafarian[1] · Ammar Al-Jodah[1] · Joshua Pinskier[1]

Abstract

This paper presents a compact flexure-based microgripper for grasping/releasing tasks. The microgripper is based on a double-stair bridge-type mechanism and consists of a bridge-type mechanism for amplifying the input displacement and the integrated parallelogram mechanisms for linearizing the motion at the microgripper jaws. The displacement transmission, amplification, linearization are accomplished in a single-stage. Stiffness modeling is established to characterize the output displacement, the displacement amplification ratio, and the input stiffness of the mechanism. The right-angle flexure hinges are utilized in the displacement amplification and transmission mechanisms to maintain the input stiffness of the mechanism. The structural design of the microgripper is optimized in such a way that a large output displacement can be achieved. Finite element analysis and experiments are conducted on the microgripper to verify the results of the analytical modeling. The proposed microgripper achieves a large output displacement of 543.8 μm with a displacement amplification ratio of 19.3. The experimental results indicate that the microgripper will be able to accommodate a grasping/releasing task.

Keywords Compliant mechanism · Piezoelectric actuator · Right-angle flexure · Microgripper

1 Introduction

A microgripper is required to perform pick, hold, and release operations. Microgrippers utilize angular grasping and parallel grasping techniques for micro-object handling tasks [1–3]. Due to the inherent advantages of parallel grasping techniques such as smooth grasping of a micro-object, no slippage, the microgrippers based on parallel grasping techniques are preferred in pick-hold-release operations.

Microgrippers have been widely used in many fields such as micromechanical assembly, microsurgery, precise robotic manipulation, and many more [4–8]. The microgripper and the multi-DOF (multiple degrees of freedom) mechanism perform together as a micromanipulator in many applications [9–12]. The microgripper plays a vital role in micro-object handling operations. The flexure-based microgripper must possess high precision, no mechanical friction, no backlash, repeatable motion, vacuum compatibility, and many more. These characteristics of the flexure-based mechanism improve the quality of micromanipulation operations. The mechanism of such flexure-based microgrippers is widely driven by piezoelectric actuators due to high force to weight ratio, fast response, high precision motion, high resonant frequency, and compact size. Further, there are other actuators such as electrostatic, electromagnetic, shaped memory alloy (SMA), electroactive polymers, and voice coil to perform micromanipulation tasks [13–15]. Further, piezoelectric actuated flexure-based mechanisms provide the required capability in achieving high precision motion and high frequency of the microgripper [16]. On the other hand, the piezoelectric actuator generates small output displacement roughly 0.1 % of its own length [17].

Prior research efforts on flexure-based microgrippers have used displacement amplification mechanisms to achieve large output displacement. Microgrippers are usually developed using symmetric and asymmetric structural design [18, 19]. Zubir et al. [20] developed a high precision flexure-based microgripper with the bias spring, which achieved a maximum output displacement of 100 μm with an amplification ratio of 2.85. Chen et al. [21] designed a

✉ Tilok Kumar Das
  tilok.das@monash.edu

1 Robotics and Mechatronics Research Laboratory,
   Department of Mechanical and Aerospace Engineering,
   Monash University, Clayton, VIC 3800, Australia

microgripper driven by hybrid actuation using a one-stage displacement amplification mechanism and achieved an amplification ratio of 3.31. Xing et al. [22] proposed asymmetric levered parallelogram mechanism-based microgripper, which obtained a displacement amplification of 4.16 and output displacement of 249.39 μm with a corresponding maximum voltage of 150V. Further, the microgrippers with multi-stage amplifications were reported to obtain large output displacement. Zhang et al. [23] proposed a monolithic compliant microgripper using two lever-type mechanisms sequentially and obtained a displacement amplification ratio of 6.0. Sun et al. [24] presented a double amplification mechanism incorporating lever-type mechanism and Scott-Russel mechanism in the microgripper and obtained a maximum jaw displacement of 134 μm with a high amplification ratio of 15.5. Liang et al. [25] proposed a monolithic piezoelectric actuated microgripper for wire clamping with an amplification ratio of 20.1 and output displacement of 140 μm, and the motion resolution of ± 0.2 μm. Shi et al. [26] developed a flexure-based microgripper using two amplifier beams and angular grasping technique and achieved a displacement amplification ratio approximately 20. Wang et al. [27] proposed a three-stage amplification mechanism based on an angular grasping technique and achieved maximum jaw motion of 190 μm with an amplification ratio of 22.6, and the motion resolution of ± 0.4 μm. However, most of the reported microgrippers use a multi-stage amplification mechanism, which induces high stiffness at the input end of the mechanism due to the stiffness of sequentially connected amplification mechanisms. Further, multi-stage displacement amplification mechanism occupies a considerable space [28]. Consequently, it limits the nominal displacement of the actuator and hinders in obtaining

a compact design. The single-stair bridge-type mechanism has the potential to obtain large output motion [29]. The double-stair, triple-stair, and multi-stair bridge-type mechanisms have the characteristics of displacement amplification and the linear output motion, as shown in Fig. 1.

In this paper, the double-stair bridge-type mechanism is utilized to develop a flexure-based piezoelectric actuated microgripper. The microgripper accomplishes the displacement amplification and linearizes the output motion in a single-stage. The analytical modeling is established and computational analysis is conducted to investigate the effect of the key design parameters on the characteristics of the microgripper. The microgripper design is optimized to provide a better understanding in terms of the displacement amplification ratio and the output displacement. The experimental studies are conducted to verify the characteristics of the microgripper.

The remaining sections of this paper are organized as follows. In Section 2, the structural design and the mechanism of the proposed microgripper are described. The characteristics of the microgripper are evaluated by analytical modeling in terms of output displacement, stiffness, stress and natural frequency in Section 3. In Section 4, the design optimization is performed to provide the better characteristics of the microgripper. In Section 5, computational analysis verifies the characteristic parameters obtained from analytical modeling. In Section 6, the FEA and analytical modeling results of the microgripper are compared to gain knowledge and understanding of the influence of the key design parameters. The experimental results of the designed microgripper are presented in Section 7. Finally, the conclusions are drawn for the proposed microgripper in Section 8.

Fig. 1 **a** Single-stair, **b** double-stair, **c** triple-stair bridge-type mechanism

(a)   (b)   (c)
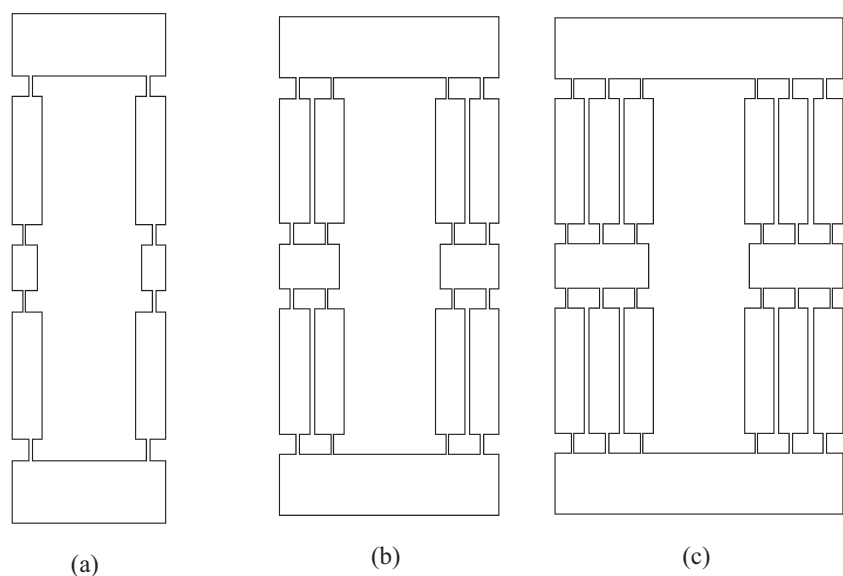
2 Mechanical design of the microgripper

Most microgrippers are designed based on configuring the displacement amplification mechanism and parallelogram mechanism serially [22, 30]. The displacement amplification mechanism magnifies the output displacement of the piezoelectric actuator. The parallelogram mechanism linearizes the output of the displacement amplification mechanism. The displacement amplification mechanism with a high amplification ratio usually generates low output stiffness. These types of displacement amplification mechanisms can not drive a parallelogram mechanism effectively to obtain large output displacement. There are microgrippers that avoid the use of a parallelogram mechanism, thus neglecting the rotation of the microgripper jaws [31, 32]. In this paper, the double-stair bridge-type mechanism is utilized to design a compliant microgripper. The mechanism consists of the properties such as amplifying the input displacement and linearizing the motion at the output ends. Figure 2 shows the CAD drawing of the proposed microgripper. The bridge-type mechanism amplifies the displacement at the input end and generates output in two directions. The parallelogram mechanisms linearize the output motion. The microgripper jaws are connected with the output ends of the mechanism. The microgripper jaws move in a closing direction while the force applied to the input end of the mechanism. This design accomplishes its grasping process on a single-stage amplification.

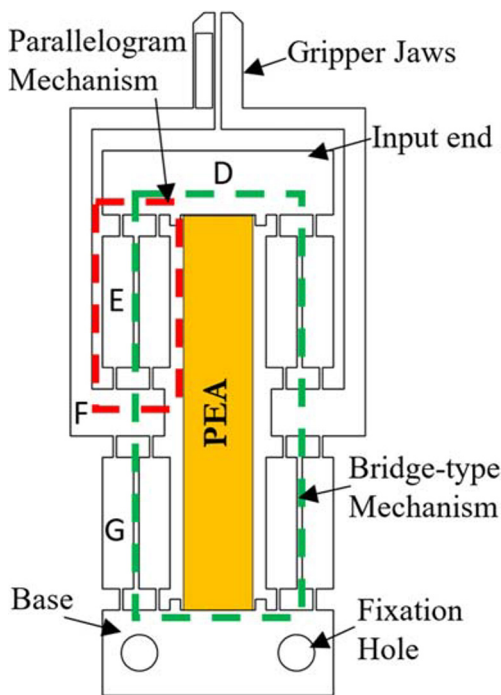Further, the microgripper uses sixteen right-angle flexural hinges. The structural design of the microgripper can utilize both circular and right-angle (leaf-type) flexural hinges. In order to avoid high input stiffness of the microgripper mechanism, the right-angle flexures are used instead of circular flexural hinges. Two types of flexural hinges with their coordinate axes namely right-angle and circular flexural hinges are shown in Fig. 3i, and Fig. 3ii, respectively. A short right-angle flexure hinge and the Pseudo Rigid Body Model are presented as shown in Fig. 3iii and Fig. 3iv, respectively. The radius of the circular flexure (r) is considered as 1 mm which is half of the length of the right-angle flexure (l). The in-plane thickness (t) and out-of-plane thickness (b) of the flexure hinges are considered as 0.3 mm and 5 mm, respectively. The translational stiffness in the x, and y-directions and rotational stiffness about the z-axis of each flexural hinges are compared in Table 1. The translational and rotational stiffness of the right-angle flexural hinge is smaller than circular flexural hinge for the same amount of applied force and moment. Thus, the input stiffness is kept low to use a small piezoelectric actuator to drive the mechanism effectively.

3 Analytical modeling

Stiffness modeling is established to calculate input stiffness, displacement amplification ratio of the microgripper. The Matrix method is applied to obtain the input stiffness and the displacement amplification ratio. Stress analysis is
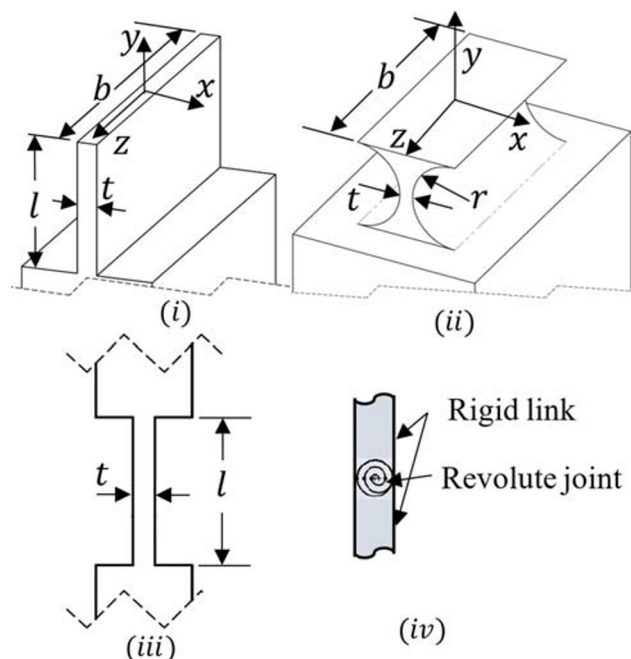

Fig. 2 CAD drawing of the microgripper design

Fig. 3 i Right-angle (leaf-type), **ii** circular flexure hinge, **iii** short right-angle flexure, and **iv** Pseudo Rigid Body Model (PRBM) of the short right-angle flexure

Table 1 Translational and rotational stiffness of each right-angle and circular flexure hinge

Stiffness	Right-angle flexure	Circular flexure
k_x, $N/\mu m$	0.3025	1.1365
k_y, $N/\mu m$	53.75	86.08
$k_{\theta z}$, Nm/rad	0.4033	1.25

Table 2 Architectural parameters of the microgripper design

Parameter	t	b	l	l_1	l_2	l_3	l_4	l_5	l_6	l_7	l_8
Unit, mm	0.3	5	2	12.3	0.6	1.25	3.4	4.4	12.3	5.65	14.3

performed to find equivalent stress and safety factor of the mechanism. Simple bending theory is utilized to find the equivalent stress. Dynamic modeling is developed to obtain the working mode frequency.

3.1 Stiffness modeling

3.1.1 Input stiffness

The input compliance and stiffness matrix of right-angle, circular, wire flexural hinges are explained to determine the translational and rotational deformation due to the applied load and moment [33]. Initially, input compliance of the microgripper at point A is calculated considering the compliance of each right-angle flexure as shown in Fig. 4a. The architectural parameters of the microgripper are presented in Table 2. The set of forces and moments, the set of translational and rotational displacements are expressed

as F and D, respectively. According to the elastic theory, the deformation twist and the loading wrench can be written as follows:

$$D = CF \tag{1}$$

$$F = KD \tag{2}$$

where C is the compliance matrix, K is the stiffness matrix and both matrices are inverse of each other. The set of translational and rotational displacement $D = [d_x \; d_y \; d_z \; \theta_x \; \theta_y \; \theta_z]^T$ and the external forces and moments $F = [F_x \; F_y \; F_z \; M_x \; M_y \; M_z]^T$. The superscript T represents the matrix transpose.

The compliance matrix for a right-angle flexure can be written as follows [34]:

$$C = \begin{bmatrix} c_1 & 0 & 0 & 0 & c_7 & 0 \\ 0 & c_2 & 0 & -c_8 & 0 & 0 \\ 0 & 0 & c_3 & 0 & 0 & 0 \\ 0 & -c_8 & 0 & c_4 & 0 & 0 \\ c_7 & 0 & 0 & 0 & c_5 & 0 \\ 0 & 0 & 0 & 0 & 0 & c_6 \end{bmatrix} \tag{3}$$

Fig. 4 **a** Microgripper architectural design **b** deformed and undeformed shape of quarter of the mechanism

(a)   (b)
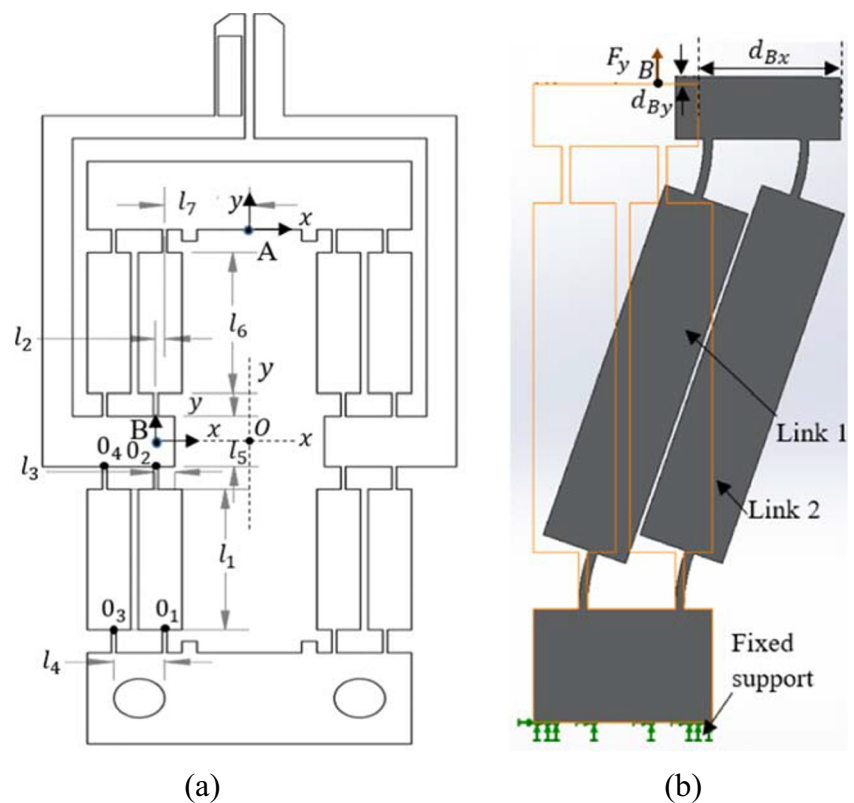
The compliance factor c_i, $(i = 1 \rightarrow 8)$ in the compliance matrix depends on the material's mechanical properties such as Young's modulus, Poisson's ratio, and right-angle flexure's architectural parameters such as thickness, width, and length. The compliance can be transferred and rotated from O_i coordinate frame to O_j coordinate frame [35].

$$C_i^j = T_i^j C_i (T_i^j)^T \tag{4}$$

where T_i^j is the 6×6 adjoint transformation matrix and it can be expressed by:

$$T_i^j = \begin{bmatrix} R_i^j & S(r_i^j)R_i^j \\ 0 & R_i^j \end{bmatrix} \tag{5}$$

where R_i^j and r_i^j are the rotation matrix and position vector. The skew-symmetric matrix S(r) for a vector $r = [r_x \; r_y \; r_z]^T$ is given by:

$$S(r) = \begin{bmatrix} 0 & -r_z & r_y \\ r_z & 0 & -r_x \\ -r_y & r_x & 0 \end{bmatrix} \tag{6}$$

The microgripper mechanism is symmetric. First, the compliance of the quarter of the design is calculated with respect to Point B. Each quarter consists of two links. The compliance of the link $O_1 \rightarrow O_2$ and $O_3 \rightarrow O_4$ with respect to point B can be obtained by:

$$C_{Link1}^B = T_1^B C_1 (T_1^B)^T + T_2^B C_2 (T_2^B)^T \tag{7}$$

$$C_{Link2}^B = T_3^B C_3 (T_3^B)^T + T_4^B C_4 (T_4^B)^T \tag{8}$$

where $C_1, C_2, C_3,$ and C_4 are the compliance matrix of flexure hinges. These compliance matrices are obtained by rotating the compliance matrix C for 90 degree counterclockwise about x-axis.

$$C_k = T_i^j C (T_i^j)^T, \; k = 1, ..., 4 \tag{9}$$

The combined compliance of both links with respect to point B can be derived by:

$$C_{Link12}^B = ((C_{Link1}^B)^{-1} + (C_{Link2}^B)^{-1})^{-1} \tag{10}$$

Due to the symmetrical structure, the compliance of other links with respect to point B can be obtained by:

$$C_{Link34}^B = \overline{R}_x(\pi) C_{Link12}^B (\overline{R}_x(\pi))^T \tag{11}$$

where

$$\overline{R}_x(\pi) = \begin{bmatrix} R_x(\pi) & 0 \\ 0 & R_x(\pi) \end{bmatrix} \tag{12}$$

Transferring the compliance of all the links from point B to point A.

$$C_{Link12}^A = T_B^A C_{Link12}^B (T_B^A)^T \tag{13}$$

$$C_{Link34}^A = T_B^A C_{Link34}^B (T_B^A)^T \tag{14}$$

The compliance of the left side of the microgripper mechanism can be obtained by:

$$C_{Left}^A = C_{Link12}^A + C_{Link34}^A \tag{15}$$

Due to the symmetry about the y-axis at point A, the right side compliance can be derived by:

$$C_{Right}^A = \overline{R}_y(\pi) C_{Left}^A (\overline{R}_y(\pi))^T \tag{16}$$

where

$$\overline{R}_y(\pi) = \begin{bmatrix} R_y(\pi) & 0 \\ 0 & R_y(\pi) \end{bmatrix} \tag{17}$$

Thus, the input compliance can be obtained by adding the stiffness of both sides and taking inverse as follows:

$$C_{in} = ((C_{Left}^A)^{-1} + (C_{Right}^A)^{-1})^{-1} \tag{18}$$

The input stiffness at point A can be obtained as follows:

$$K_{in} = (C_{in})^{-1} \tag{19}$$

3.1.2 Displacement amplification ratio

The amplification mechanism is symmetric to the left and right with respect to point O and about the y-axis, and the left side of the mechanism is symmetric to up and down and about the x-axis. Therefore, a quarter of the mechanism is considered for finding the displacement amplification of the amplification mechanism, as shown in Fig. 4b. Assuming the base with fixed support, the output compliance at point B is obtained by:

$$C_{Link12}^B = ((C_{Link1}^B)^{-1} + (C_{Link2}^B)^{-1})^{-1} \tag{20}$$

where C_{Link1}^B and C_{Link2}^B are the compliance of the link 1 and 2 with respect to the point B. The displacement of the point B in the x and y direction due to the force in the y direction can be obtained by:

$$d_{Bx} = C_{Link12}^B(2, 1) \tag{21}$$

$$d_{By} = C_{Link12}^B(2, 2) \tag{22}$$

The amplification of the mechanism on the left side can be obtained by:

$$\lambda_{amp} = \frac{d_{out}}{d_{in}} = \frac{C_{Link12}^B(2, 1)}{2C_{Link12}^B(2, 2)} \tag{23}$$

3.2 Stress analysis

The applied force at the input end of the mechanism creates a bending moment in the right-angle flexure rotation axis. Bending stress is induced due to the moment about the rotation axis of right-angle flexure. Applying the simple bending theory and assuming no stress concentration at the

outer edges of the flexure, the bending stress can be written as follows [36]:

$$\sigma_b = \frac{Et}{2l}\phi_1 \tag{24}$$

where ϕ_1 is the rotation of leaf-type flexure hinge. Assuming a PRRP (P: prismatic, and R: revolute) mechanism and the PRBM approach, a quarter of the mechanism can be presented, as shown in Fig. 5. The rotation angle of the flexure hinges can be calculated as follows [37]:

$$\phi_1 = \theta_1' - \theta_1 = cos^{-1}(\frac{l_8 - d_{in}/2}{L}) - cos^{-1}(\frac{l_8}{L}) \tag{25}$$

Further, maximum tensile stress is induced in the thinnest portion of the leaf-type flexure when the translational deformation occurs. The tensile stress can be obtained by:

$$\sigma_t = \frac{F_{in}}{A_{min}} = \frac{K_{in}d_{in}}{bt} \tag{26}$$

where A_{min} is the cross-sectional area of the right-angle flexure hinges. The safety factor of the mechanism can be calculated from Eq. 27.

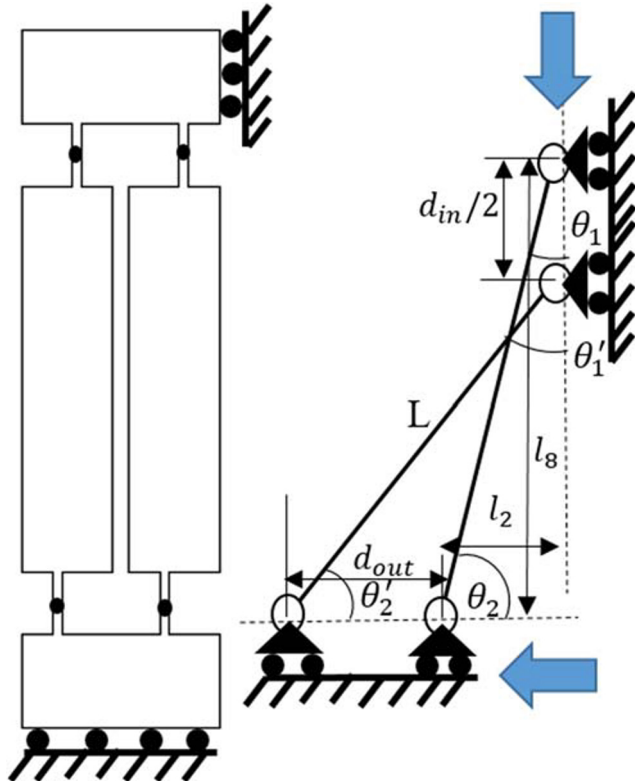$$\eta_{SF} = \frac{yield\ strength}{allowable\ stress} \tag{27}$$

Fig. 5 Rotation of the flexures hinge based on PRBM approach and PRRP mechanism

3.3 Dynamical modeling

Dynamic modeling is established to predict the working mode frequency of the microgripper. Lagrange's equation is given by:

$$\frac{d}{dt}\left(\frac{\partial T}{\partial \dot{q}}\right) - \frac{\partial T}{\partial q} + \frac{\partial V}{\partial q} = F_i \tag{28}$$

where q is the generalized parameters. T and V are the kinetic and potential energies, respectively. F_i is the non-conservative force.

The kinetic energy equation of the microgripper can be derived as:

$$\begin{aligned} T = & \frac{1}{2}m_D\dot{d}_{in}^2 + \frac{1}{2}m_F\left\{\left(\frac{\dot{d}_{in}}{2}\right)^2 + \dot{d}_{out}^2\right\} \times 2 \\ & + \frac{1}{2}m_E\left\{\left(\frac{3\dot{d}_{in}}{4}\right)^2 + \left(\frac{\dot{d}_{out}}{2}\right)^2\right\} \times 4 + \frac{1}{2}I_E\dot{\theta}_E^2 \times 4 \\ & + \frac{1}{2}m_G\left\{\left(\frac{\dot{d}_{in}}{4}\right)^2 + \left(\frac{\dot{d}_{out}}{2}\right)^2\right\} \times 4 + \frac{1}{2}I_G\dot{\theta}_G^2 \times 4 \end{aligned} \tag{29}$$

where the second moment of mass of the link is expressed as $I = \frac{mL^2}{12}$, the rotation angle can be presented aproxiamately $\theta_E = \theta_G = \frac{d_{out}}{L}$, the output displacement is obtained from input and output displacement relations as $d_{out} = \lambda_{amp} \times d_{in}$.

$$V = 8 \times \frac{1}{2}k_\theta(\theta_E^2 + \theta_G^2) \tag{30}$$

where the rotational stiffness, $k_\theta = \frac{Ebt^3}{12l}$. Substituting the kinetic and potential energies Eq. (29) and Eq. (30) into Eq. 28, the equivalent mass and stiffness can be obtained as follows:

$$M = m_D + (\frac{5}{2} + \frac{8}{3}\lambda_{amp}^2)m_E + (\frac{1}{2} + 2\lambda_{amp}^2)m_F$$

$$K = \frac{16k_\theta\lambda_{amp}^2}{L^2}$$

The natural frequency of the microgripper designed microgripper can be obtained from Eq. 31.

$$f_n = \frac{1}{2\pi}\sqrt{\frac{K}{M}} \tag{31}$$

4 Design optimization

The key design parameters of the microgripper are selected, which influence the characteristics of the microgripper. The design optimization is conducted to investigate the effect of key design parameters of the microgripper. The stiffness of the piezoelectric actuator has a high impact on the microgripper design optimization. The properties of the

piezoelectric actuator (model: PK4FYC2, from Thorlabs, Inc.) are considered. The objectives and constraints for optimizing the microgripper design are set as follows:

1) Maximize the output displacement and the displacement amplification ratio
2) The architectural parameters to be optimized: l, t, l_2
3) Subject to

      a) Input stiffness $\leq 20\% K_p$
      b) Equivalent stress $\leq \sigma_y$
      d) Parameter ranges: $1mm \leq l \leq 3mm$; $0.2mm \leq t \leq 0.5mm$; $0.5mm \leq l_2 \leq 1mm$

where K_p is piezoelectric actuator's stiffness, σ_y is the yield strength of the material Al 7075-T651. The parameter ranges depend on the material properties, manufacturing limitation, input stiffness, and safety factor. Applying the analytical modeling for the microgripper the displacement amplification ratio, input stiffness, natural frequency, and equivalent stress are obtained. The equivalent stress value remains lower than the yield strength of the material. The optimum design is proposed with key parameters l= 2 mm, t = 0.3 mm, l_2 = 0.6 mm. The total displacement amplification ratio, input stiffness, and working mode frequency of the microgripper are obtained as 20.44, 4.136 $N/\mu m$, and 402.8 Hz, respectively.

5 Computational analysis

The characteristics of the designed microgripper were evaluated using finite element analysis in ANSYS Workbench 18.0. The physical and mechanical properties of Al 7075-T651 material are utilized for the structural design of the microgripper and to perform the finite element analysis. The relevant properties of Al 7075-T651 material are density 2.81 g/cm^3, modulus of elasticity 71.7 GPa and tensile strength at yield point 503 MPa. The computational analysis is conducted in terms of output displacement for determining the displacement amplification ratio in the grasping direction. The material failure is estimated with equivalent (Von-Mises) stress and sufficient safety factor is maintained to handle repeated tasks of micromanipulation.

5.1 Output displacement analysis

The displacement amplification ratio of the microgripper is obtained from input and output displacement relationship of the mechanism. In static structural analysis, a displacement of 30 μm was applied on the input end of the bridge-type mechanism of PEA position, and the deformed shape of each jaw was obtained as shown in Fig. 6a. The FEA result showed that the maximum deformation in each jaw of the microgripper was 301.9 μm. A total of 603.8 μm displacement can be achieved for the two jaws of the microgripper, which represents the displacement amplification ratio of the microgripper is 20.1. Fig. 6b shows that the parasitic motion along the y-axis is 15.45 μm. Thus, the maximum parasitic motion in the y-direction is approximately 5.1% of the motion in the x-direction. Further, there was a less significant amount of rotation of jaw around z-axis, which was less than 8.41×10^{-5} radian. The microgripper can be used for
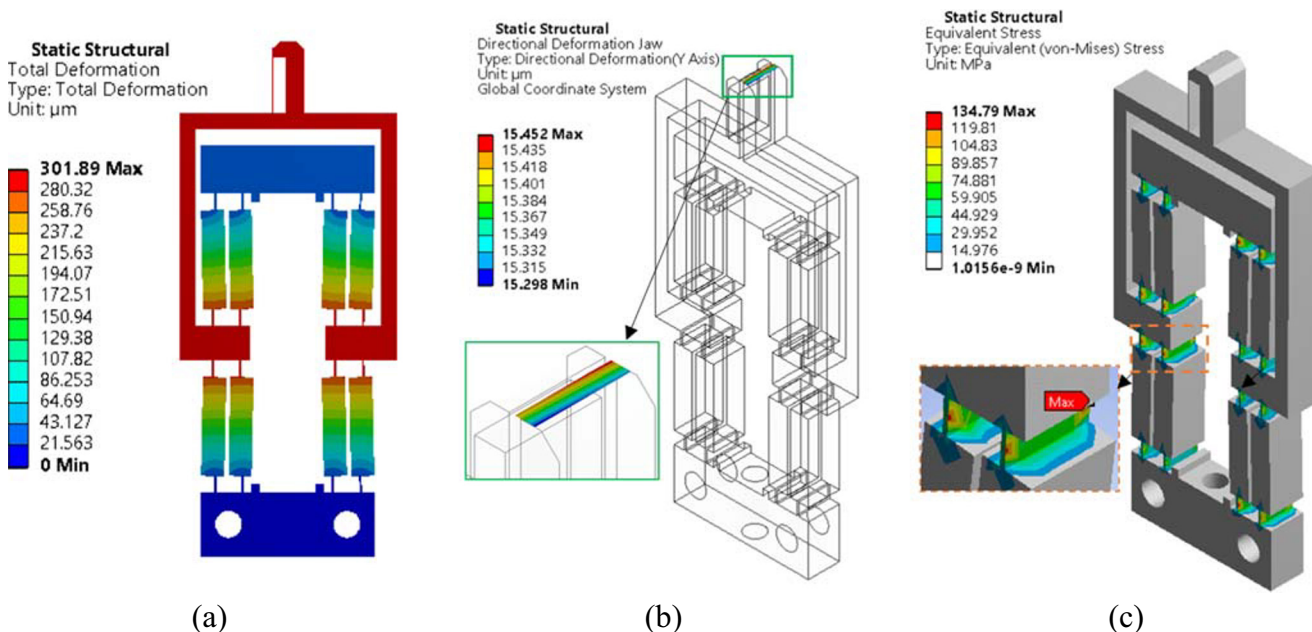

Fig. 6 **a** Displacement of gripper jaws, **b** parasitic motion of jaws, and **c** equivalent stress
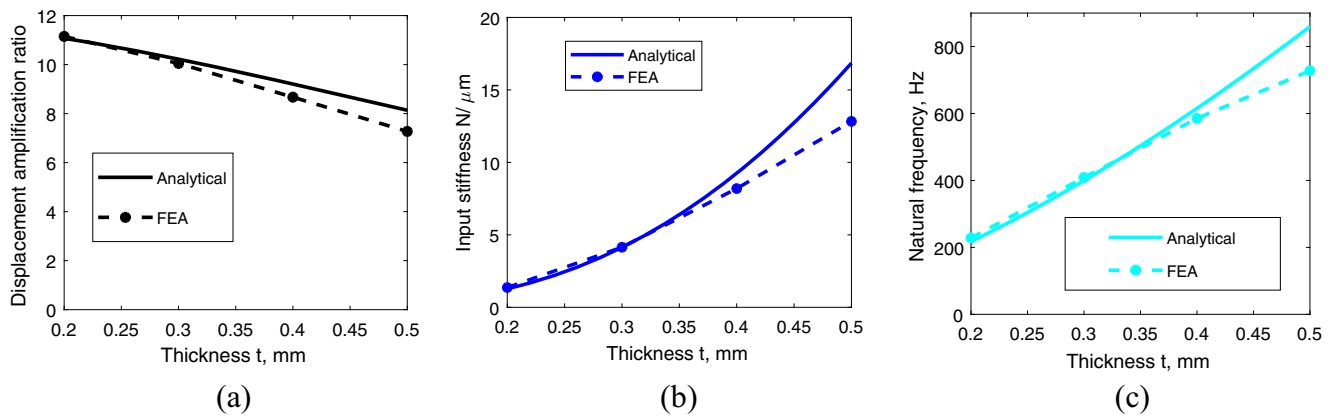
Fig. 7 Relationship between thickness t, and **a** displacement amplification ratio, **b** input stiffness, **c** natural frequency

coarse positioning a micro-object in micromanipulation systems.

5.2 Stiffness analysis

In the stiffness analysis, 1 N force is applied at the input end of the mechanism and the corresponding displacement is obtained. The input stiffness of the mechanism is calculated from the displacement and force relationship. The input stiffness of the mechanism is 4.11 N/μm.

5.3 Stress analysis

The stress analysis was performed in the FEA simulation. The maximum equivalent (Von-Mises) stress of the micro-gripper was 134.79 MPa while the displacement of 30 μm is applied at the input end of the mechanism. The Von-Mises stress was significantly less than the tensile strength at the yield point of the material. The stress induces in the middle section of each right-angle flexural hinges as shown in Fig. 6c. The safety factor of the microgripper is calculated by using Eq. 27. The minimum safety factor was obtained as 3.73 in the worst-case scenario. Further, the working mode

frequency of the microgripper was found as 408.7 Hz from the modal analysis.

6 Comparisons with analytical method

The results of the analytical modeling and finite element analysis are compared in this section. Finite element analysis is conducted on microgripper designs for varying key design parameters of the microgripper. Further, the results of the analytical modeling are obtained as discussed in Section 3. The analytical and finite element analysis results are provided through Figs. 7, 8 and 9.

Figure 7 shows that the displacement amplification ratio decreases gradually with the increase of the thickness of the flexure hinges. The input stiffness and natural frequency rise sharply with the increase of thickness of the flexure hinges. Figure 8 shows that the length of flexure hinges was sensitive for the input stiffness of the mechanism. There was a slight impact on the amplification ratio of the mechanism while varying the length (l) of the flexure hinges. Figure 9 shows that the displacement amplification ratio and input stiffness of the mechanism decreases gradually when the
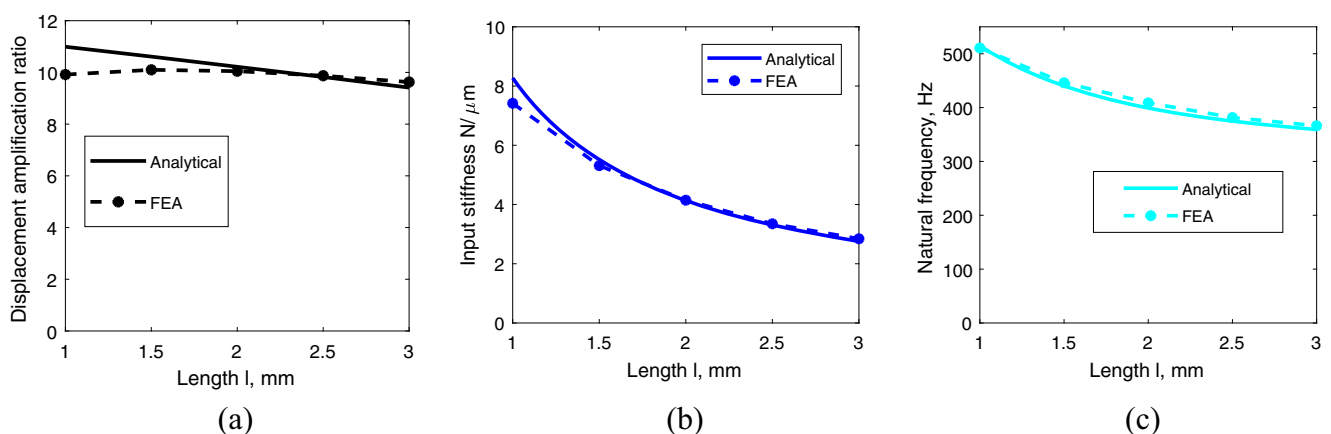

Fig. 8 Relationship between length l, and **a** displacement amplification ratio, **b** input stiffness, **c** natural frequency
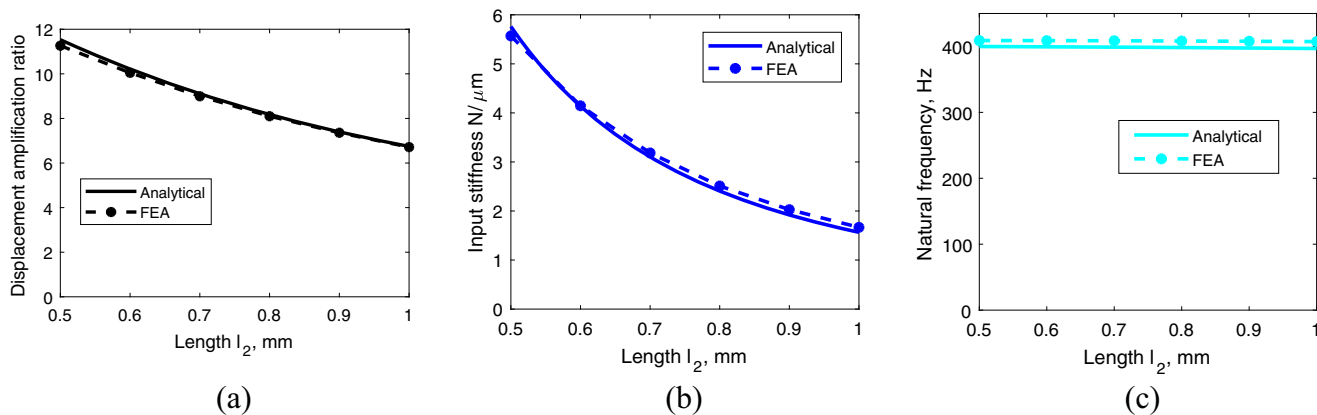
Fig. 9 Relationship between length l_2, and **a** displacement amplification ratio, **b** input stiffness, **c** natural frequency

length (l_2) increases. The natural frequency has a negligible effect on varying the length (l_2). The maximum deviation of each parameter of the microgripper for entire ranges is provided in Table 3.

Further, the results are presented in 3-dimensional coordinates to illustrate the effect of two parameters variation simultaneously. Figure 10 shows that the displacement amplification ratio increases while the thickness (t) and length (l) of the right-angle flexural hinge are reduced. The natural frequency and the input stiffness of the mechanism rise sharply with the increase of thickness (t) and decrease of length (l) of the flexure hinges. Figure 11 depicts that the desired output such as the displacement amplification ratio is increasing, and input stiffness of the mechanism is decreasing while the thickness (t) of the flexural hinge and the length (l_2) between the flexural hinges are reduced together. Conversely, the desired natural frequency reduces due to varying the parameters for the same trend. Figure 12 illustrates that the desired output such as the displacement amplification ratio and the natural frequency are increasing while both the length (l) of the flexural hinge and the length (l_2) between the flexural hinges are reduced simultaneously. Contrarily, the input stiffness also is increasing for the same condition.

7 Experiments

The microgripper is fabricated from a piece of Al 7075-T651 material using wire electric discharge machining

(WEDM), as shown in Fig. 13a. The experimental setup of the microgripper was prepared for actuation tasks, control computation, data acquisition and analysis in the real-time system as shown in Fig. 13b–c. The piezoelectric actuator is embedded in the microgripper design. The experimental investigation was conducted for measuring displacement with a two-axis laser interferometry-based measurement system [38, 39]. Two high-stability plane mirror interferometers (HSPMI) are positioned and aligned with a beam splitter, fold mirror, and reflector to measure the input and output displacement of the mechanism.

Open-loop experiment The embedded piezoelectric actuator of the microgripper was driven with a periodic sine wave with 0.2 Hz and an amplitude of 150V in the open-loop experiment. The maximum output displacement of a jaw can reach 271.9 μm as shown in Fig. 14. The microgripper achieves a total output displacement of 543.8 μm for a corresponding input displacement of 28.15 μm. The experimental results show that the microgripper has a displacement amplification ratio of 19.3. The area efficiency of the microgripper [40] is obtained as the ratio of the output displacement to the area of the mechanism and is expressed as:

$$Area\ efficiency = \frac{output\ displacement}{area} \qquad (32)$$

The significance of the area efficiency is that the contribution of one square millimeter area of the microgripper to generate output displacement. According to this parameter, the microgripper is as efficient as to generate 315.2 nm

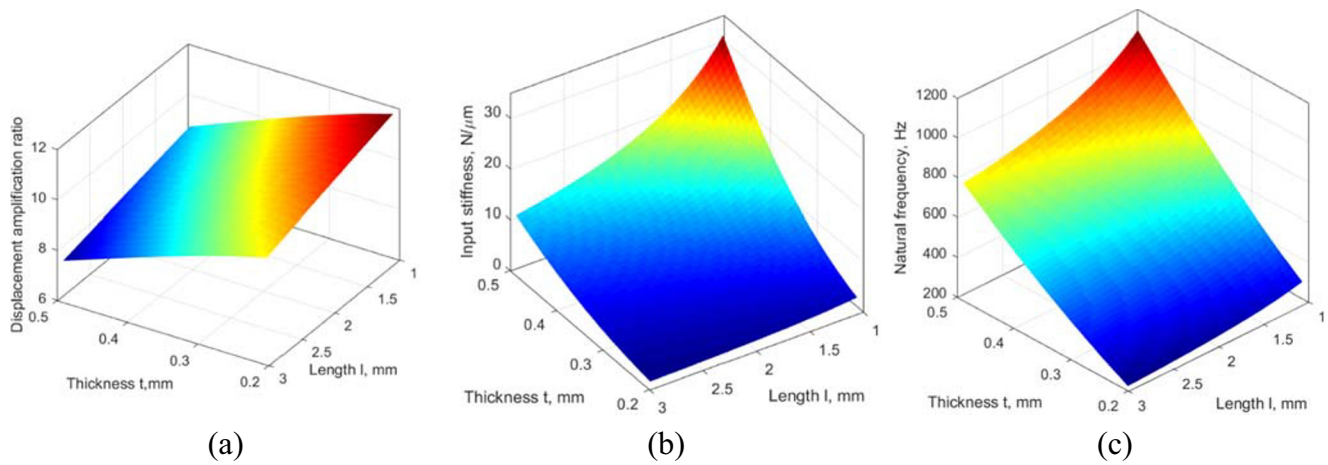| Table 3 Deviation between analytical and FEA results for entire parameter range			
Item/Deviation (%)/Parameter	Thickness (t)	Length (l)	Length (l_2)
Displacement amplification ratio	11.8	10.8	2.4
Input stiffness, $N/\mu m$	34	11.5	3.5
Natural frequency, Hz	18	6.8	4.3

Fig. 10 a Displacement amplification ratio, **b** input stiffness, **c** natural frequency with respect to thickness (t) and length (*l*) of the right-angle flexural hinge
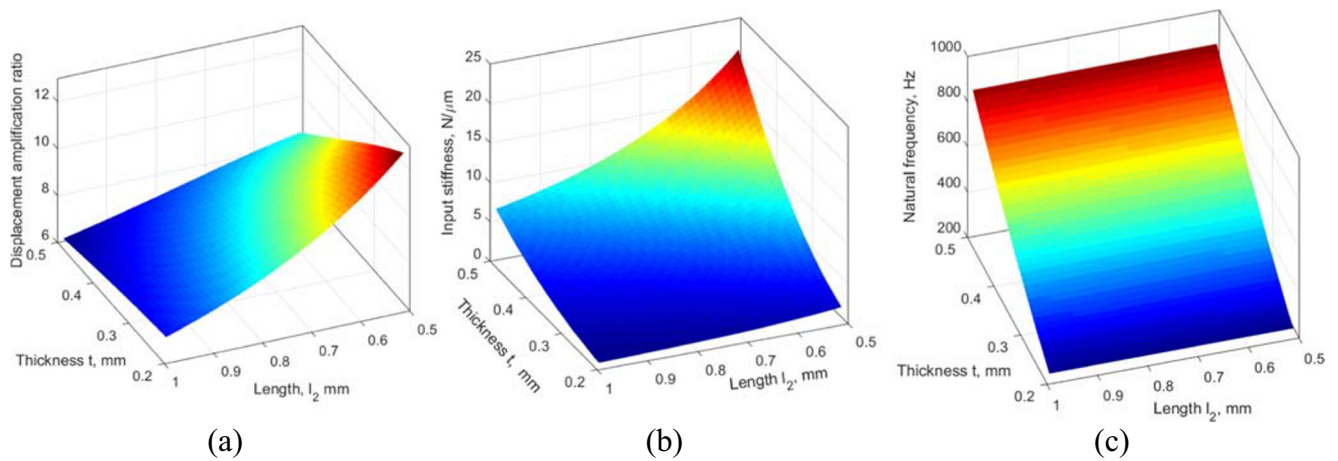

Fig. 11 a Displacement amplification ratio, **b** input stiffness, **c** natural frequency with respect to thickness (t) and length (*l₂*) between the right-angle flexural hinges
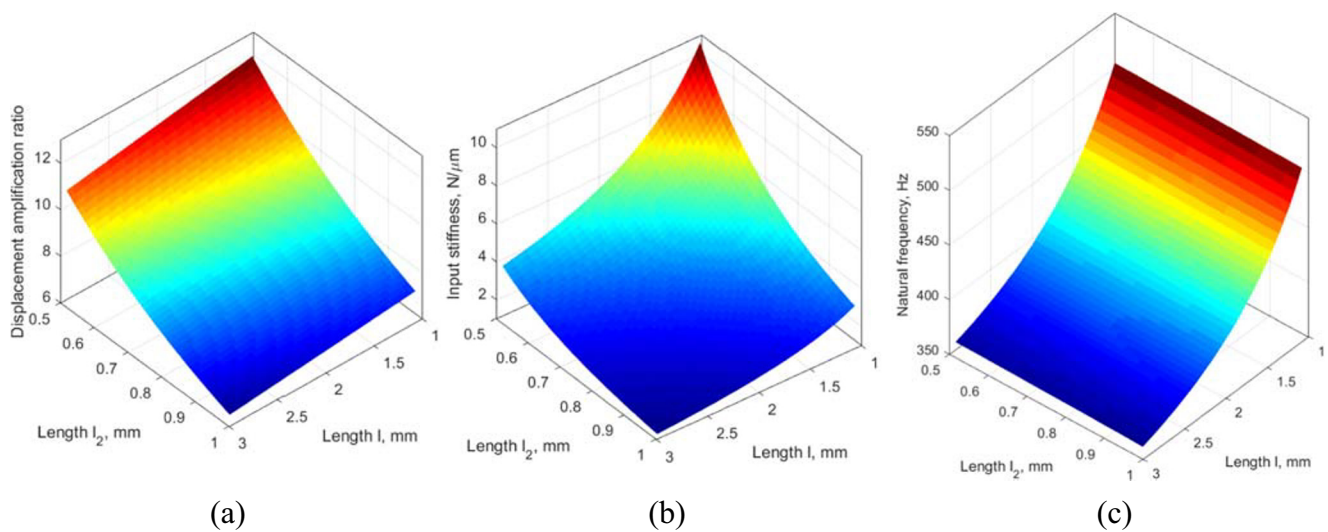

Fig. 12 a Displacement amplification ratio, **b** input stiffness, **c** natural frequency with respect to length (*l*) of the right-angle flexural hinges and length (*l₂*) between the right-angle flexural hinges
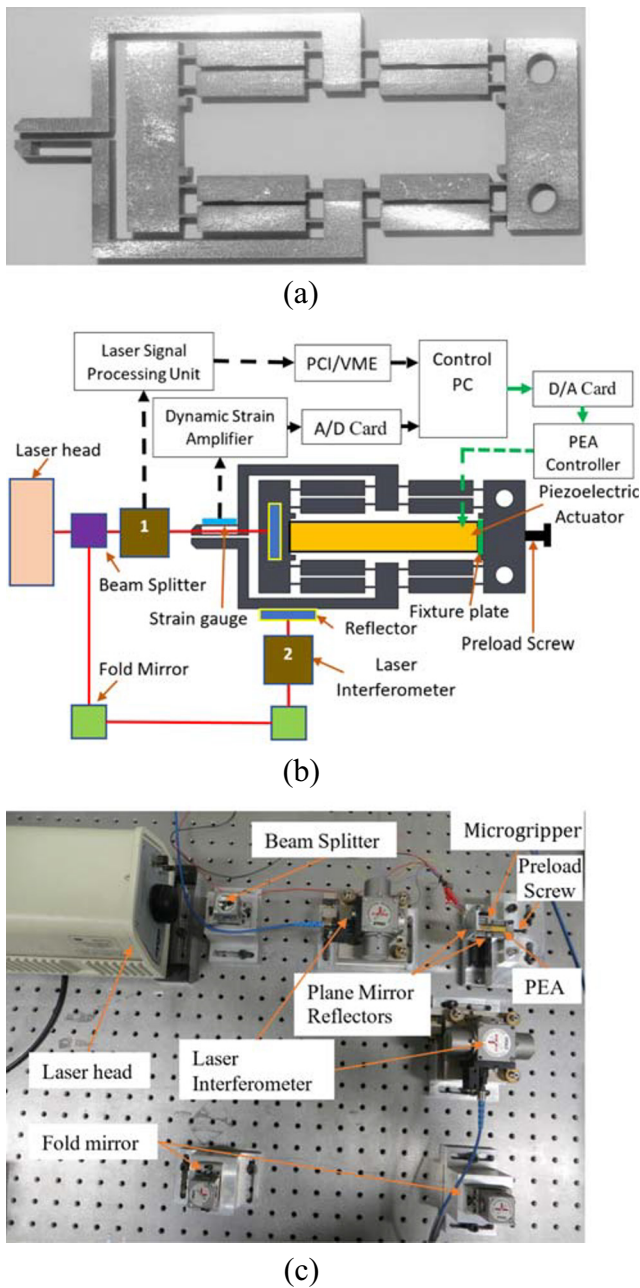
(a)

(b)

(c)

Fig. 13 **a** Photograph of the fabricated microgripper, **b** block diagram of the experimental setup for the open-loop and closed-loop system and **c** photograph of the experimental setup.

output displacement from one square millimeter area of the microgripper. Further, the hysteresis effect of the piezoelectric actuator was apparent in the input voltage vs input and output displacement relationship, as shown in Fig. 14.

Closed-loop experiment The closed-loop experiments were conducted to examine trajectory tracking performance and motion resolution of the microgripper. The Proportional Integral (PI) control strategy was utilized to investigate the tracking error and motion resolution. A periodic sine
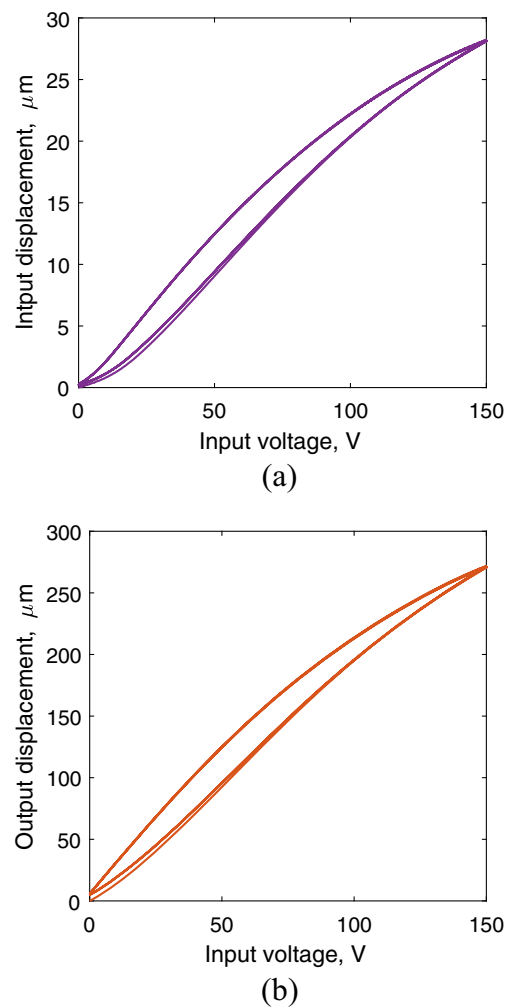

(a)

(b)

Fig. 14 **a** Input displacement vs input voltage, **b** output displacement vs input voltage

wave with 0.2 Hz and an amplitude of 200 μm was implemented on the microgripper. The PI control scheme parameters are $K_p = 0.00001$, and $K_i = 0.05$. The results of the Proportional Integral (PI) control scheme are displayed in Fig. 15. The mechanism of the microgripper with the Proportional Integral (PI) control technique capable of reducing the root mean square error (RMSE) to 215 nm, which is 0.11 % of the amplitude of the sine-wave.

In order to achieve the motion resolution of the microgripper, a small stair signal of 30 nm for 2 seconds each step was provided to the PI control scheme. The desired and actual step responses are presented in Fig. 16. The steady-state error is maintained within ± 15 nm. A high precision motion resolution was achieved using the PI control technique.

Grasping a micro-object A strain gauge was attached to the surface of one jaw, as shown in Fig. 17a. It was used as a force sensor to measure the gripping force.
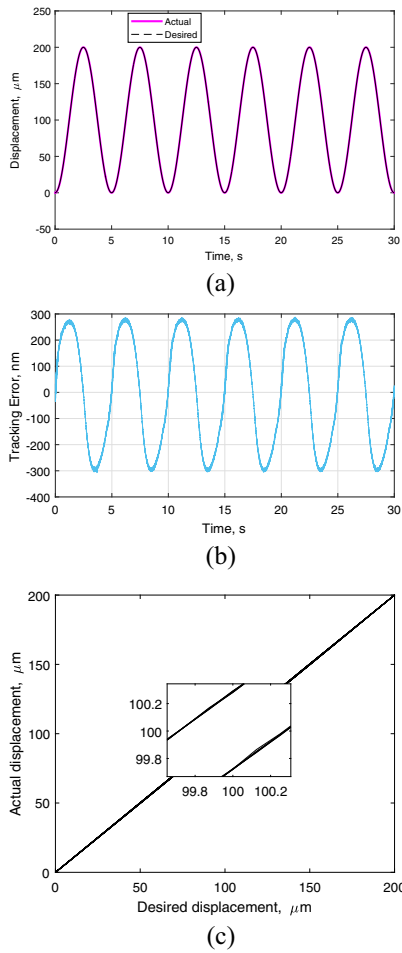
Fig. 15 **a** Output displacement of the microgripper jaws with respect to time, **b** tracking error, **c** actual displacement versus desired displacement

The strain gauge (model: KFGS-2-350-C1-23, Kyowa Electronic Instruments Co., Ltd.) was calibrated using a
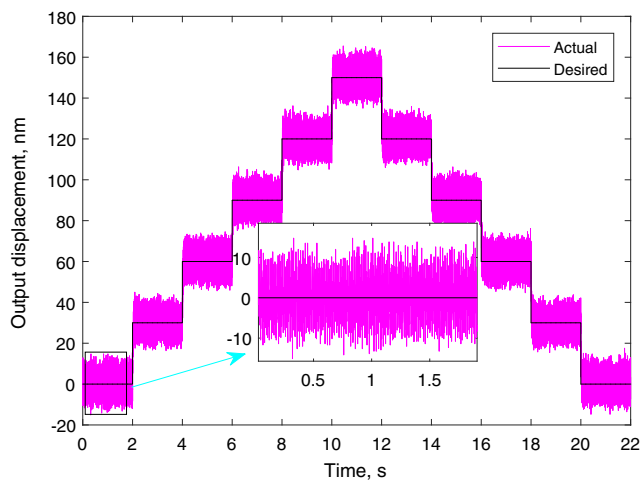

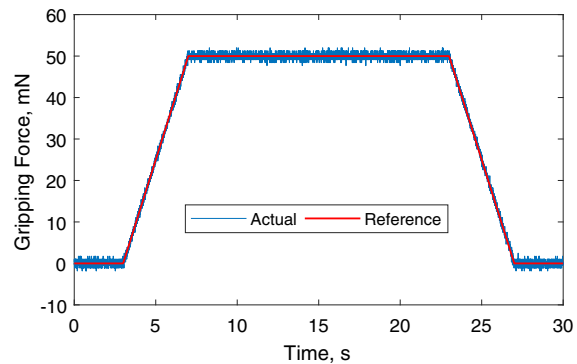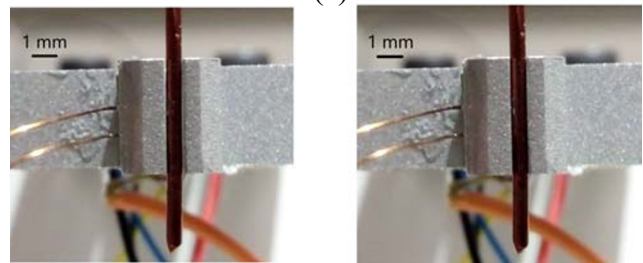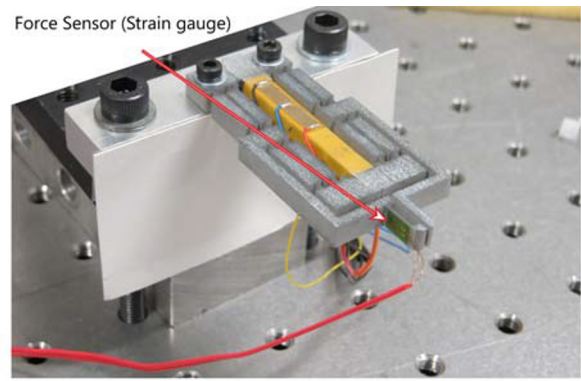**Fig. 16** Motion resolution of step response

Fig. 17 **a** Force sensor (strain gague) in the microgripper, **b** before grasping the metal wire, **c** while holding the metal wire, and **d** force response plot

10.5 mN weight to the jaw. The resulted voltage was recorded with a dynamic strain amplifier (model: YE3817, SINOCERA Piezotronics, Inc.). The voltage and force relationship was obtained as 2.352 mN/mV. A micro-object (metal wire of 700 μm diameter) was utilized to grasp and verify its ability to perform grasping/releasing tasks, as shown in Fig. 17b–c. A force feedback control loop was

Table 4 Proposed microgripper's characteristics

Parameter	Analytical	FEA	Experiment
Total amplification ratio	20.44	20.1	19.3
Total output displacement (μm)	575.39	565.82	543.8

Table 5 Performance comparison of the piezoelectric actuated microgrippers

Reference	Size mm × mm	Stage	Amplification Ratio	Output Displacement, μm	Area Efficiency, nm/mm^2
Zubir et al. [20]	50 × 30	single	2.85	100	66.67
Sun et al. [24]	40 × 35	two	15.5	134	95.72
Wang et al. [27]	50 × 27	three	22.6	190	140.74
Feng et al. [41]	80 × 35	two	20	202	72.14
Yang et al. [42]	110 × 58	two	21.4	213.9	33.53
This work	63.90 × 27	single	19.3	543.8	315.2

developed with a proportional-integral control strategy. The constant gains of the proportional-integral control strategy were set as $K_p = 1$, and $K_i = 15$. A trapezoidal reference signal with an amplitude of 50 mN force was applied to grasp the metal wire and the desired output force was obtained, as shown in Fig. 17d.

The proposed microgripper characteristics are shown in Table 4. The analytical modeling and FEA method result of the total displacement amplification ratio and output displacement deviates from the experimental result by 5.91% and 4.15 %, respectively. The proposed microgripper derived from optimization is well estimated and the percentages of the deviation are in the acceptable range. Further, the performance of the microgripper is compared with the previously reported microgrippers, as presented in Table 5. The developed microgripper shows good performance in terms of the characteristics such as displacement amplification ratio, the output displacement, and area efficiency. Further, the characteristics of the microgripper indicate that the proposed design can be applied in the micromanipulation systems. To conclude, the compact design of the microgripper outperforms in terms of large output displacement and high displacement amplification ratio with a single-stage displacement amplification mechanism.

8 Conclusion

A compact flexure-based piezoelectric actuated microgripper is proposed in this paper. The mechanism of the microgripper utilizes a double-stair bridge-type mechanism. The microgripper achieved a large output displacement and high displacement amplification ratio by a single-stage amplification mechanism. The single-stage amplification mechanism assists in achieving a compact design. The short right-angle flexure hinges are used to form the displacement amplification and transmission mechanisms. The analytical modeling was established to optimize and to characterize the effect of the design parameters of the microgripper. The computational analysis was used to compare and verify the analytical

model results. The experimental result showed that thepro-posed microgripper achieved a large output displacement of 543.8 μm with a displacement amplification ratio of 19.3. The microgripper achieved a high precision motion resolution of $\pm$ 15 nm. It is anticipated from the analysis that the microgripper will be able to perform repeated micro-object handling tasks without failure.

References

1. Vidyaa V, Kanthababu M, Thilagar SH, Balasubramanian R (2018) Evaluation of macro sized metal based microgrippers for handling microcomponents. Precis Eng 54:403–411
2. Zubir MNM, Shirinzadeh B, Tian Y (2009) A new design of piezoelectric driven compliant-based microgripper for micromanipulation. Mech Mach Theory 44(12):2248–2264
3. Raghavendra MR, Kumar AS, Jagdish BN (2010) Design and analysis of flexure-hinge parameter in microgripper. Int J Adv Manuf Tech 49(9):1185–1193
4. Zhong Y, Shirinzadeh B, Alici G, Smith J (2006) Soft tissue modelling through autowaves for surgery simulation. Med Biol Eng Comput 44(9):805–821
5. Gu GY, Zhu LM, Su CY, Fatikow S, Ding H (2015) Proxy-based sliding-mode tracking control of piezoelectric-actuated nanopositioning stages. IEEE/ASME Transactions on Mechatronics 20(4):1956–1965
6. Qin Y, Shirinzadeh B, Tian Y, Zhang D (2013) Design issues in a decoupled XY stage: Static and dynamics modeling, hysteresis compensation, and tracking control. Sensors and Actuators A: Physical 194:95–105
7. Zimmermann S, Tiemerding T, Fatikow S (2015) Automated robotic manipulation of individual colloidal particles using vision-based control. IEEE/ASME Transactions on Mechatronics 20(5):2031–2038
8. Tian Y, Shirinzadeh B, Zhang D (2009) A flexure-based mechanism and control methodology for ultra-precision turning operation. Precis Eng 33(2):160–166
9. Wang P, Xu Q (2017) Design of a flexure-based constant-force XY precision positioning stage. Mech Mach Theory 108:1–13
10. Pinskier J, Shirinzadeh B (2019) Topology optimization of leaf flexures to maximize in-plane to out-of-plane compliance ratio. Precis Eng 55:397–407

11. Fung RF, Lin WC (2009) System identification of a novel 6-DOF precision positioning table. Sensors and Actuators A: Physical 150(2):286–295

12. Clark L, Shirinzadeh B, Bhagat U, Smith J, Zhong Y (2015) Development and control of a two DOF linear – angular precision positioning stage. Mechatronics 32:34–43

13. Boudaoud M, Haddab Y, Le Gorrec Y (2013) Modeling and optimal force control of a nonlinear electrostatic microgripper. IEEE/ASME Transactions on Mechatronics 18(3):1130–1139

14. López-Walle B, Gauthier M, Chaillet N (2008) Principle of a submerged freeze gripper for microassembly. IEEE Trans Robot 24(4):897–902

15. Lin CM, Fan CH, Lan CC (2009) A shape memory alloy actuated microgripper with wide handling ranges. In: IEEE/ASME International conference on advanced intelligent mechatronics

16. Tian Y, Shirinzadeh B, Zhang D, Liu X, Chetwynd D (2009) Design and forward kinematics of the compliant micro-manipulator with lever mechanisms. Precis Eng 33(4):466–475

17. Qi KQ, Xiang Y, Fang C, Zhang Y, Yu CS (2015) Analysis of the displacement amplification ratio of bridge-type mechanism. Mech Mach Theory 87:45–56

18. Somà A, Iamoni S, Voicu R, Müller R (2018) Design and experimental testing of an electro - thermal microgripper for cell manipulation. Microsyst Technol 24(2):1053–1060

19. Liang C, Wang F, Shi B, Huo Z, Zhou K, Tian Y, Zhang D (2018) Design and control of a novel asymmetrical piezoelectric actuated microgripper for micromanipulation. Sensors and Actuators A: Physical 269:227–237

20. Zubir MNM, Shirinzadeh B (2009) Development of a high precision flexure-based microgripper. Precis Eng 33(4):362–370

21. Chen W, Zhang X, Fatikow S (2016) A novel microgripper hybrid driven by a piezoelectric stack actuator and piezoelectric cantilever actuators. Rev Sci Instrum 87(11):1–11

22. Xing Q, Ge Y (2015) Parametric study of a novel asymmetric micro-gripper mechanism. J Adv Mech Des Syst Manuf 9(5):1–12

23. Zhang D, Zhang Z, Gao Q, Xu D, Liu S (2015) Development of a monolithic compliant SPCA-driven micro-gripper. Mechatronics 25:37–43

24. Sun X, Chen W, Tian Y, Fatikow S, Zhou R, Zhang J (2013) A novel flexure-based microgripper with double amplification mechanisms for micro / nano manipulation. Rev Sci Instrum 84(8):1–10

25. Liang C, Wang F, Tian Y, Zhao X, Zhang H, Cui L, Zhang D, Ferreira P (2015) A novel monolithic piezoelectric actuated flexure-mechanism based wire clamp for microelectronic device packaging. Rev Sci Instrum 86(4):1–10

26. Shi Q, Yu Z, Wang H, Sun T, Huang Q, Fukuda T (2018) Development of a highly compact microgripper capable of online calibration for multisized microobject manipulation. IEEE Trans Nanotechnol 17(4):657–661

27. Wang F, Liang C, Tian Y, Zhao X, Zhang D (2016) Design and control of a compliant microgripper with a large amplification ratio for high-speed micro manipulation. IEEE/ASME Transactions on Mechatronics 21(3):1262–1271

28. Chen W, Zhang X, Li H, Wei J, Fatikow S (2017) Nonlinear analysis and optimal design of a novel piezoelectric-driven compliant microgripper. Mech Mach Theory 118:32–52

29. Choi KB, Lee JJ, Kim GH, Lim HJ, Kwon SG (2018) Amplification ratio analysis of a bridge-type mechanical amplification mechanism based on a fully compliant model. Mech Mach Theory 121:355–372

30. Zubir MNM, Shirinzadeh B, Tian Y (2009) Development of novel hybrid flexure-based microgrippers for precision micro-object manipulation. Rev Sci Instrum 80(6):1–14

31. Wang F, Liang C, Tian Y, Zhao X, Zhang D (2015) Design of a piezoelectric-actuated microgripper with a three-stage flexure-based amplification. IEEE/ASME Transactions on Mechatronics 20(5):2205–2213

32. Yang YL, Lou JQ, Wu GH, Wei YD, Fu L (2018) Design and position / force control of an S-shaped MFC microgripper. Sensors and Actuators A: Physical 282:63–78

33. Qin Y, Shirinzadeh B, Zhang D, Tian Y (2013) Compliance modeling and analysis of statically indeterminate symmetric flexure structures. Precis Eng 37(2):415–424

34. Koseki Y, Tanikawa T, Koyachi N, Arai T (2000) Kinematic analysis of translational 3-DOF micro parallel mechanism using matrix method. IEEE/RSJ International Conference on Intelligent Robots and Systems 1:786–792

35. Li Y, Xu Q (2009) Design and analysis of a totally decoupled flexure-based XY parallel micromanipulator. IEEE Trans Robot 25(03):645–657

36. Smith ST (2000) Flexure-elements of elastic mechanisms. CRC Press, Boca Raton

37. Zubir MNM, Shirinzadeh B, Tian Y (2009) Development of a novel flexure-based microgripper for high precision micro-object manipulation. Sensors and Actuators A: Physical 150(2):257–266

38. Bhagat U, Shirinzadeh B, Clark L, Qin Y, Tian Y, Zhang D (2014) Experimental investigation of robust motion tracking control for a 2-DOF flexure-based mechanism. IEEE/ASME Transactions on Mechatronics 19(6):1737–1745

39. Qin Y, Shirinzadeh B, Tian Y, Zhang D, Bhagat U (2014) Design and computational optimization of a decoupled 2-DOF monolithic mechanism. IEEE/ASME Transactions on Mechatronics 19(3):872–881

40. Tang H, Li Y (2015) A new flexure-based $Y\theta$ nanomanipulator with nanometer-scale resolution and millimeter-scale workspace. IEEE/ASME Transactions on Mechatronics 20(3):1320–1330

41. Feng F, Cui Y, Xue F, Wu L (2012) Design of a new piezo-electric micro-gripper based on flexible magnifying mechanism. Applied Mechanics and Materials 201-202:907–911

42. Yang YL, Wei YD, Lou JQ, Tian G, Zhao XW, Fu L (2015) A new piezo-driven microgripper based on the double-rocker mechanism. Smart Mater Struct 24(7):1–11